Check for updates

Analysis of local velocity gradients in rapid mixer using particle image velocimetry technique

N.-S. Park and H. Park

Department of Civil Engineering, Korea Advanced Institute of Science and Technology (KAIST), Daejeon, Korea

Abstract Recognizing the significance of factual velocity fields in a rapid mixer, this study focuses on analyzing local velocity gradients in various mixer geometries with particle image velocimetry (PIV) and comparing the results of the analysis with the conventional *G*-value, for reviewing the roles of *G*-value in the current design and operation practices. The results of this study clearly show that many arguments and doubts are possible about the scientific correctness of *G*-value, and its current use. This is because the *G*-value attempts to represent the turbulent and complicated factual velocity field in a jar. Also, the results suggest that it is still a good index for representing some aspects of mixing condition, at least, mixing intensity. However, it cannot represent the distribution of velocity gradients in a jar, which is an important factor for mixing. This study as a result suggests developing another index for representing the distribution to be used with the *G*-value.

Keywords *G*-value; local velocity gradient; particle image velocimetry (PIV); rapid mixing

Introduction

Camp and Stein (1943) developed the *G*-value, mean velocity gradient, assuming that the product of shear rate and shear stress at a point is the same as the power per unit volume in rapid mixer and other coagulation–flocculation basins. Since then, it has been widely accepted that the mixing conditions with the same *G*-value are almost identical from the coagulation point of view. For almost 50 years, researchers, designers and operators of water treatment facilities have considered the *G*-value as an important index representing the overall mixing intensity and the dissipation of energy in rapid mixer, as well as coagulation–flocculation process and it has been widely used in the design and scale-up of mixing process components (AWWA, 1990; Liem *et al*., 1999).

Since the middle of the 1980s, some research results have been published that criticize and question the use of the *G*-value as a valid basis for the design of flocculation basins. Oldsue (1983) stated that the G-value cannot provide information about the shear rate distribution in a coagulation–flocculation tank, and different performances are expected from different impellers at the same *G*-value. Cleasby (1984) said that the *G*-value is only valid for eddies whose sizes are smaller than those necessary for flocculation in both water and wastewater treatments. Clark (1985) also criticized the use of the parameters of absolute velocity gradient and root mean square (RMS) velocity gradient for three-dimensional flow since Camp and Stein (1943) derived them with the assumptions in two dimension. Han and Lawler (1992) stated that the importance of the velocity gradient (*G*-value) has been apparently overemphasized in the traditional view of flocculation, based on rectilinear models for collision frequency functions and the consideration of uniformly sized particles. Wu and Patterson (1989) and Stanley and Smith (1995) measured the variability of turbulence and mixing levels in a jar test tank using Laser Doppler Velocimetry (LDV). Due to a limitation of LDV that it can measure the temporal change at a point but not the spatial change at a time, they suggested that only the local velocity gradient may be quite different from the *G*-value. In recognition of the limitation of LDV, Cheng *et al*. (1997) measured the factual

Water Science and Technology: Water Supply **Vol 2 No 5–6 pp 47–55** © IWA Publishing 2002

Downloaded from http://iwaponline.com/ws/article-pdf/2/5-6/47/407882/47.pdf
by guest

velocity field in a 2 l square jar using particle image velocimetry (PIV) and stated that the *G*-value cannot properly represent the spatial and temporal heterogeneity of mixing.

In summary, these critics say that the *G*-value cannot properly represent the actual hydrodynamic conditions in mixing and can thus only be applied to limited conditions. This leads to a suggestion that it cannot be used as a major parameter for design and operation of mixer and coagulation–flocculation as has been used so far. It has been strongly doubted that the *G*-value can be a scaling factor between the lab scale jar test and the field application, say, in determining an optimum coagulant dose.

On the other hand, it is known that the PIV technique can measure the velocity of an entire flow field instantaneously to quantitatively reveal global structures of a complicated and unsteady flow. It has been mainly applied in the fields of fluid dynamics and only a few applications are reported in the fields of water and wastewater treatment (Rajendran and Patel, 2000; Cheng *et al*., 1997). Recent technological advancement in optics and computer technology, which have resolved the problems of storage space and camera frequency, has enhanced the potential. For example, a stereoscopic PIV technique is now being used to measure the velocity component in three dimensions (Image Information Technology Co., 2000).

Using this advanced technology of PIV, this study is to examine the differences in velocity fields in different shapes of mixer and to evaluate whether the *G*-value can represent the differences in velocity field. In the end, we extend the results to discuss the adequacy of the G-value as used for design and operation of mixer and coagulation–flocculation up until now. For that, we conduct jar tests with three different shapes of jar at various *G*-values and analyze the velocity fields of some of the jar tests using PIV techniques. PIV data are used to calculate local velocity gradients, which cannot be obtained by any other traditional measurement techniques, for comparison with *G*-values and discussion.

Material and methods

Jar tests

The jar tests are carried out with kaolin dispersion (initial turbidity: 5.70 NTU) and three different jars. The jars are made of acrylic and their effective volume for experiment is 2 l, as shown in Figure 1. We use three different types of jar for our study: a circular jar with squared-baffles, a circular jar with no baffle, and a Hudson jar with no baffle. A 2

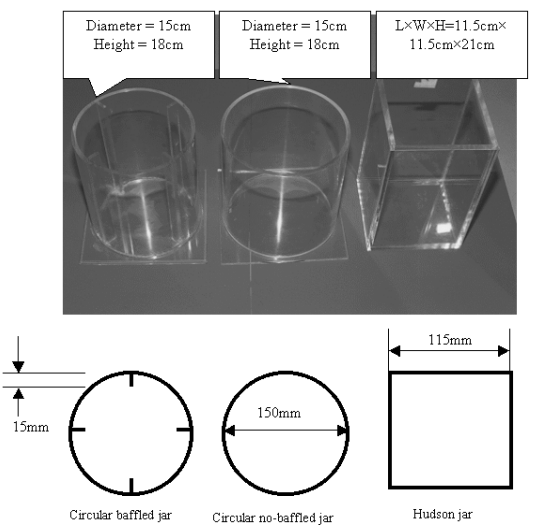

Figure 1 Three different shapes of jar for jar tests

Downloaded from http://iwaponline.com/ws/article-pdf/2/5-6/47/407882/47.pdf
by guest

flat-bladed stainless steel impeller is used for these jar tests. This impeller consists of two vertically mounted blades and a rotating vertical shaft. The inner and outer radii of the blades are 3 mm and 38.1 mm, respectively. The width of the blades is 15 mm.

Artificial raw water is made by mixing kaolin with distilled water, adding alkalinity of 2 meq/L with sodium bicarbonate (Andreu-Villegas and Letterman, 1976). Its pH is then adjusted with acetic acid to an optimal value of 7.1 after the addition of coagulant (Gorden, 1991). The procedure of the jar tests is also as follows. Sample water for each test is made by mixing 1,900 mL of distilled water, 80 mL of kaolin stock suspension, 20 mL of sodium bicarbonate, and 3 mL of acetic acid (5% v/v). Turbidities in all tests are measured in NTU with the Hach 2100N turbidmeter whose accuracy is up to 0.01NTU. The rapid mixing time of 15 s is chosen to limit any possibility of flocculation, as the conventional jar test suggests 15–60 s for rapid mixing (Gorden, 1991; Purchas, 1977).

Hudson and Wolfner (1967) recommended to mix coagulant with bulk in as short a time as possible. After rapid mixing, the impeller rotating speed is set at 50 rpm for 15 minutes. After 10 minutes of settling, a sample of approximately 20 mL is taken from 20 mm below the surface for measurement. The optimal pH and coagulant dose for turbidity removal with aluminum sulfate ($Al_2[SO_4]3\ 18H2O$) for kaolin dispersion, which are determined by this procedure, are 5 ppm and 7.1, respectively. These values are applied for all tests.

Each shape of mixer is tested at 12 different impeller speeds. They are 125, 150, 175, 200, 250, 275, 300, 325, 350, 375 and 400 revolutions per minute (rpm). The *G*-values in different types of mixers are different from each other at the same impeller speeds.

Methodology of PIV analysis

For the most proper mixing conditions, under which residual turbidity was the lowest in each jar from the previous jar tests, PIV analysis is applied to measure factual velocity fields and to calculate local velocity gradients from point to point in jars for a comparison with conventional *G*-values.

The PIV system was developed as a quantitative flow visualization device. It uses an optical imaging technique to measure velocities simultaneously at many points in a flow field (Cheng *et al*., 1997; Rajendran and Patel, 2000). A laser sheet which is generated by expanding a laser beam with a combination of cylindrical and spherical lenses illuminates a planar flow region. Seeding particles must be sufficiently small and non-buoyant to follow fluid motion. Therefore, poly-vinyl chloride (PVC) is used as seeding particle (Rajendran and Patel, 2000). This material has a similar density (1.05 g/mL) to water, which is desirable in relating the particle motion to the water velocity. The motion of the seeding particle is then captured by a recording device, such as a charge-coupled device (CCD) camera. As shown in Figure 2, the PIV system used in this study consists of an argon laser, high speed CCD camera, lenses, controller, host computer (Pentium III 650 MHz, 120 Mbytes RAM) and PIV software. The PIV software uses an auto-correlation technique to find the displacement of particles before plotting the vectors in a uniform grid. An interrogation area of 362 $\times$ 362 pixels is chosen and the velocity vectors are plotted on the image in a 40×30 grid.

The relative positions for viewing area in each jar are side planar including the impeller as shown in Figure 3. At each case, 60 consecutive images are recorded at a second interval. The measured vector data provides the information about velocity fields at a grid of 1,200 points (40×30 points in the *X*, *Y* plane) per image. The step size of D*x* is about 3.7 mm in the *X*-direction and that of Δy is about 4.8 mm in the *Y*-direction. In order to derive local velocity gradients from the factual vector data, as can be seen from Figure 3, three vertical grid lines are chosen: the first ($x1$), the second ($x2$) and the third ($x3$) lines are located at 18.4, 55.2 and 73.6 mm away from the *Y*-axis, respectively. Local velocity gradient in each case is calculated by dividing the factual velocity difference (du) with the spatial difference (dy)

Downloaded from http://iwaponline.com/ws/article-pdf/2/5-6/47/407882/47.pdf
by guest

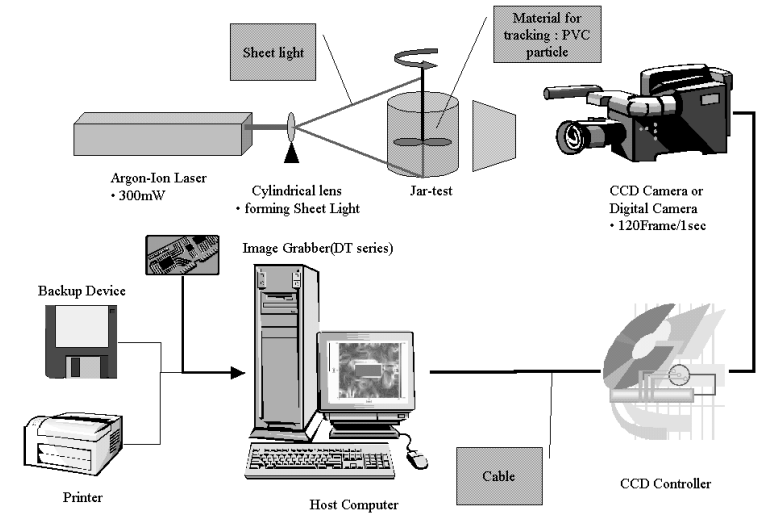

Figure 2 Schematic of the PIV system used in this study

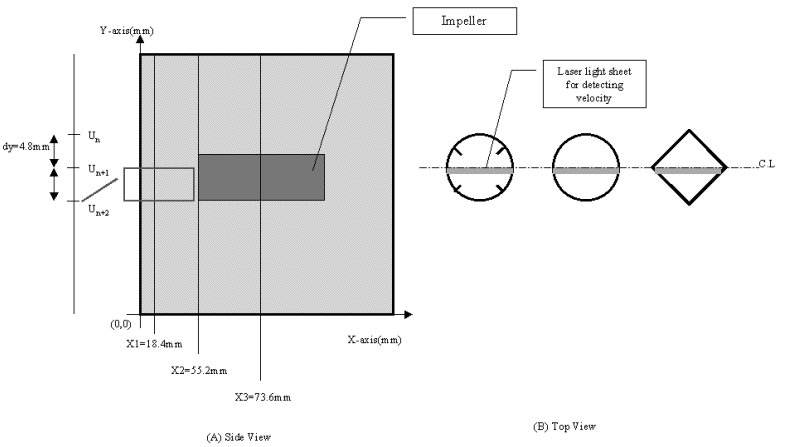

Figure 3 Coordinate systems used for viewing area: (a) side view; (b) top view

between two adjacent points on a vertical grid line. In order to investigate the sensitivity of local velocity gradients to dy, six different spatial differences are used: 4.8, 9.6, 14.4, 19.2, 24.0 and 28.8 mm.

Results and discussion

Results of jar tests

Figure 4 shows residual turbidities in NTU with the three jars. In the circular no-baffled jar, a residual turbidity of 0.45 NTU is the lowest at a rotating speed of 250 rpm of which the *G*-value is 108.1s^{-1}. (They are called here the optimum rotating speed and *G*-value, respectively.)

As the rotating speed and *G*-value increase further, the residual turbidity also increases. In the circular baffled jar, the optimum rotating speed and *G*-value are 200 rpm and 131.7 s^{-1}, respectively, at which the residual turbidity is 1.28 NTU. Also, in the Hudson jar, they are 150 rpm and 147 s^{-1} with a residual turbidity of 1.11 NTU. It is noted that the optimum rotating speeds and *G*-values in different jars are not identical.

The residual turbidity at the optimum *G*-value is the lowest in the circular no-baffled jar,

Downloaded from http://iwaponline.com/ws/article-pdf/2/5-6/47/407882/47.pdf
by guest

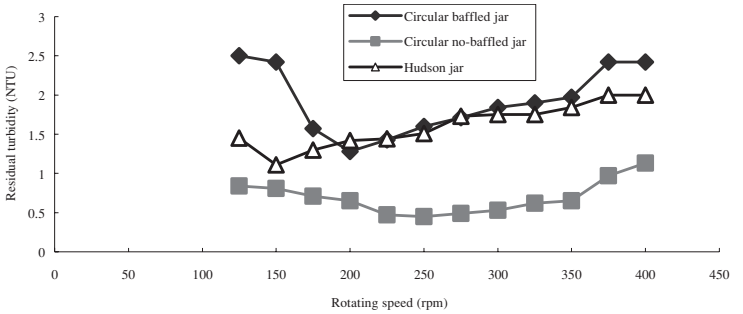

Figure 4 Comparison of residual turbidity (NTU)

the middle in the Hudson jar and the highest in the circular baffled jar. In addition, the optimum G-value in the circular no-baffled jar is the lowest among them, which is 108.1 s^{-1}. This indicates that the baffles in a mixer and the hexahedron shape do not improve the dispersal of coagulant at all and, in turn, ultimate turbidity removal. This result is a good match with that emphasized by Oldsue (Oldsue, 1983). He said that, in the case of mixing fluids of low viscosity, baffles in a mixer increase the power consumption by the impeller but decrease the overall general motion of fluid in the mixer. In particular, he discussed "over-baffling phenomenon".

Results of PIV analysis

Figure 5 shows the results of PIV analysis in terms of velocity contour. The circular baffled jar case at 200 rpm of rotating speed (G-value = 131.7 s^{-1}) is shown in Figure 5a, the

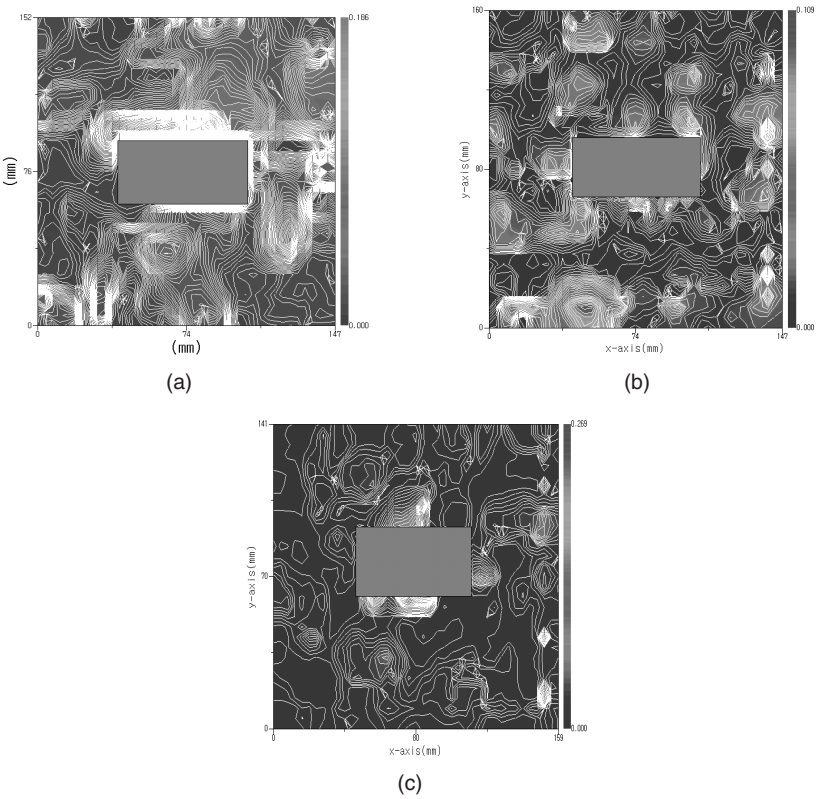

Figure 5 Results of PIV analysis: (a) circular baffled jar; (b) circular no-baffled jar; (c) Hudson jar

Downloaded from http://iwaponline.com/ws/article-pdf/2/5-6/47/407882/47.pdf
by guest

circular no-baffled jar case at 250 rpm (G-value = 108.1 s^{-1}) in Figure 5b, and Hudson jar case at 150 rpm (G-value = 147.8 s^{-1}) in Figure 5c.

As shown in Figure 5, each figure is identical to the one that is displayed on a computer monitor, using the velocity measured at 1,200 points (40 × 30 points in the X, Y plane). It shows a vector velocity field superimposed on the particle images. An ASCII data file in a grid format is also produced for further flow analysis. Using these data files, we derive local velocity gradients in each case by dividing the factual velocity differences (du) with each of the six spatial displacements (dy = 4.8, 9.6, 14.4, 19.2, 24.0 or 28.8 mm), as previously discussed.

Figure 6 shows the distribution of local velocity gradients on the three lines of $x1$, $x2$ and $x3$ in the three jars when dy is 4.8 mm. Since the portion of the rotating impeller is set as an obstacle in which velocities are zero, velocity gradients in which the impeller is located (y = about 70–90 mm) become zero.

Table 1 shows the statistical results of the local velocity gradients with various spatial displacements, using their averages and standard deviations, to summarize what is shown in Figure 6. In general, the averages and standard deviations of the local velocity gradients become smaller as the spatial difference (dy) increases from 4.8 mm to 28.8 mm. When we look at the case of dy = 4.8 mm, the Hudson jar yields the highest average of 7.93 s^{-1} and the largest standard deviation of 7.51 on the $x1$ line, while the circular baffled jar has an average value of 4.67 s^{-1} and a standard deviation of 4.38, and the circular no-baffled jar has 5.84 s^{-1} and 6.31, respectively. On the $x2$ line, the circular no-baffled jar produces the highest average of 9.15 s^{-1} and the largest standard deviation of 11.40. On the $x3$ line, the circular no-baffled jar also yields the highest average and the largest standard deviation. Even for the other cases with different spatial differences, similar results occur, that is, the highest average and the largest standard deviation are obtained in the Hudson jar on the $x1$ line and in the circular no-baffled jar on the $x2$ and $x3$ lines.

In both the circular baffled (Figure 5a) and Hudson jar (Figure 5c) cases, the average values on the $x1$ line are highest, and those on the $x2$ line are lowest. On the other hand, in the circular no-baffled jar (Figure 5b), the average values on the $x2$ line are highest, and those

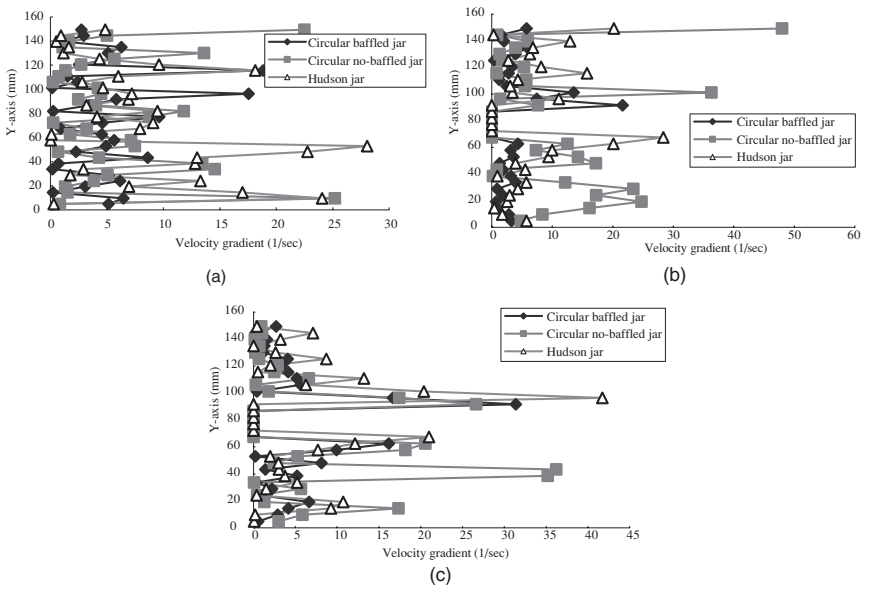

Figure 6 Comparison of local velocity gradients when dy = 4.8 mm: (a) on the $x1$ line; (b) on the $x2$ line; (c) on the $x3$ line

Downloaded from http://iwaponline.com/ws/article-pdf/2/5-6/47/407882/47.pdf
by guest

on the $x1$ line are lowest. These differences indicate that the mixer shape influences the distribution of local velocity gradients. Particularly, baffles in a mixer and hexahedron shape make the velocity gradients near the sidewalls increase. It can be said that the dissipations of supplied mechanical energy are relatively concentrated on the sidewalls in baffled or hexahedron shaped mixers, compared to the no-baffled case. This also explains the results that local velocity gradients only near sidewalls in Hudson jar are higher than those in the other cases.

A higher average and a larger standard deviation of velocity gradients indicate a higher intensity and a wider fluctuation of turbulence resulting in better mixing in a jar. Since the better mixing of the Hudson jar on the $x1$ line, mainly due to its hexahedron shape, is only limited in the vicinity of the sidewalls, the circular no-baffled jar which shows better mixing on the $x2$ and $x3$ lines can be said to yield overall the best mixing among the three jars. In addition to the best distribution of stronger turbulence (white-colored areas), this suggests that the circular no-baffled jar provides most proper mixing conditions and, as a result, the lowest residual turbidity in jar test.

As shown in the last row of Table 1, the conventional G-values by Camp and Stein (1943) are 131.7, 108.1 and 147.8 s^{-1} for the three jars, respectively, which are larger by an order of magnitude than the velocity gradients calculated from PIV analysis. As we know, the gradient is a function of length of dy. In the above calculation, the smallest one that we can get from the PIV analysis is 4.8 mm. This has led us to question the gradients at smaller lengths than 4.8 mm, considering that the sizes of small turbulent eddies can be a couple of micrometres.

For investigating this conjecture in details, we plot average values with their dy and derive three trend lines as shown in Figure 7. All trend lines have correlation factors (R^2 values) larger than 0.99. As shown in Figure 7 and the table next to it, an average value larger than 100 s^{-1} starts to occur at about 36 μm in the circular baffled jar case, at about 1.0 μm in the circular no-baffled case and at 154 μm in the Hudson jar case. These results indicate that the real G-values of hundreds are possible at the smaller lengths, even though it is impossible to verify due to technical limitations. The fact that some real turbulent eddies can have such sizes, we think also supports that the G-value in fact represents the magnitude of velocity gradients with certain sizes of turbulence, even though not covering the whole range of sizes. In fact, since it is almost impossible to get the magnitude of velocity gradients for a whole range of turbulent eddy sizes, we think G-value can be an index of the gradients, at least, for real design and operation.

Table 1 Comparison between local velocity gradients and conventional G-value. Note: August is average value, SD is standard deviation

dy(mm)		Circular baffled (s^{-1})			Circular no-baffled (s^{-1})			Hudson (s^{-1})		
		x1	*x2*	*x3*	*x1*	*x2*	*x3*	*x1*	*x2*	*x3*
4.8	Avg.	4.67	3.35	4.40	5.84	9.15	6.88	7.93	6.35	5.99
	SD	4.38	4.36	6.61	6.31	11.40	10.53	7.51	6.94	8.78
9.6	Avg.	3.99	2.53	2.99	4.98	7.74	5.69	6.82	4.84	4.81
	SD	3.08	2.73	3.41	4.28	8.30	8.22	5.78	4.27	4.78
14.4	Avg.	3.41	1.85	2.44	4.13	7.12	5.22	5.91	3.65	3.98
	SD	2.41	1.74	2.44	4.85	6.82	10.02	5.21	3.24	3.39
19.2	Avg.	3.03	1.39	2.04	3.92	6.48	4.75	5.36	2.91	3.27
	SD	1.92	1.31	1.89	2.59	5.79	5.71	4.75	2.31	2.56
24.0	Avg.	2.47	1.18	1.58	3.68	5.96	4.18	4.83	2.24	2.63
	SD	1.40	1.07	1.45	2.23	4.96	4.82	4.28	1.67	2.20
28.8	Avg.	1.85	1.10	1.38	3.42	5.45	3.64	4.30	1.72	2.16
	SD	1.14	0.96	1.25	2.05	4.27	4.05	3.86	1.28	1.86
Conventional G-value (s^{-1})			131.7			108.1			147.8	

Downloaded from http://iwaponline.com/ws/article-pdf/2/5-6/47/407882/47.pdf
by guest

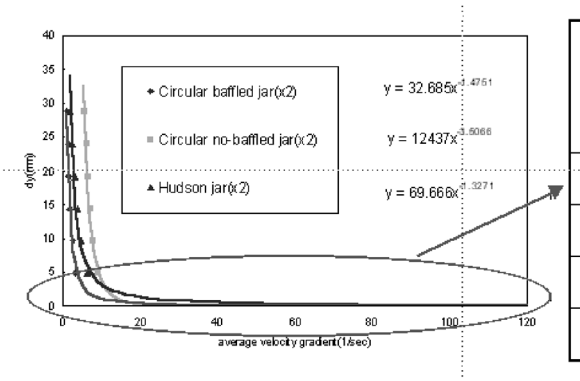

dy(μm)	Avg. value(s^{-1})		
	Circular baffled	Circular no-baffled	Hudson
154	37.8	25.1	100.1
36	100.1	38.0	299.7
1.0	1149.1	105.5	4459.9
0.6	1624.7	122.0	6553.8

Figure 7 Magnitude of velocity gradients with various d*y* (the length of spatial displacement) on *x*2 line

On the other hand, since the conventional *G*-value is defined as mean value by root-mean-square velocity gradient (Cleasby, 1984), it cannot give any information about the spatial distribution of local velocity gradients in a mixer, which is important in mixing. Of course, it cannot show the kind of difference happening in the vicinity of sidewalls in different shapes of jar, as shown in Figure 6 and Table. 1. This limitation is obvious since the *G*-value is based on the assumption that the product of shear rate and shear stress at a point equals power per unit volume (Oldsue, 1983).

Conclusions

As a result, this study concludes as follows.

- From the comparison of *G*-value and local velocity gradients (refer to Table 1 and Figure 7), even though the *G*-value may be inaccurate, it is a practically decent index for representing the magnitude of mixing intensity. Simply since the *G*-value has no concept about the size of turbulent eddies from point to point in mixers, it looks much different from factual velocity gradients. However, for turbulent eddies of small size, as discussed above, the *G*-value reasonably represent the magnitude of velocity gradients.
- On the other hand, the *G*-value cannot represent the distribution of the factual velocity field in a mixer, which is another important factor in mixing. We think another index representing the distribution needs to be developed to work with the *G*-value.
- This study has demonstrated that mixing and its hydrodynamics in a mixer should be understood in depth for proper use of the jar test. PIV techniques, as well as computational fluid dynamics, are thought to be used for investigating the details of the turbulence in relation with mixing, as used in other research (Levecq *et al*., 2001; Park *et al*., 2003; Park and Park, 2002).

References

Andreu-Villegas, R. and Letterman, R.D. (1976). Optimizing flocculator power input. *Journal of Environmental Engineering, ASCE*, **102**(2), 251–263.

AWWA (1990). *Water Quality and Treatment*. American Water Works Association, McGraw-Hill Book Co., New York, USA.

Camp, T.R. and Stein, P.C. (1943). Velocity gradient and internal work in fluid motion. *Journal of Boston Society of Civil Engineers*, **30**(4), 210–237.

Cheng, C.Y., Atkinson, J.F. and Bursik, M.I. (1997). Direct measurement of turbulence structures in mixing jar using PIV. *Journal of Environmental Engineering, ASCE*, **123**(2), 115–125.

Clark, M.M. (1985). Critique of Camp and Stein's RMS velocity gradient. *Journal of Environmental Engineering, ASCE*, **111**(6), 741–754.

Cleasby, J.L. (1984). Is velocity gradient a valid turbulent flocculation parameter? *Journal of Environmental Engineering, ASCE*, **100**(5), 875–897.

Downloaded from http://iwaponline.com/ws/article-pdf/2/5-6/47/407882/47.pdf
by guest

Gorden, L.M. (1991). Turbulence intensity of mixing relation to flocculation. *Journal of Environmental Engineering, ASCE*, **117**(6), 731–748.

Han, M. and Lawler, D.F. (1992). The (relative) insignificance of G value in flocculation, *Journal of American Water Works Association*, **84**(10), 79–91.

Hudson, H.E. and Wolfner, J.P. (1967). Design of mixing and sedimentation basins. *Journal of American Water Works Association*, **59**(10), 1257–1268.

Image Information Technology Co., Ltd. (2000). *CACTUS2000 manual*, IIT Co., Ltd.

Levecq, C., Essemiani, K. and De Traversay, C. (2001). Hydraulic study and optimization of water treatment processes using numerical simulation. *Preprints of 2001 IWA Conference*, 15–17 October, Berlin, Germany.

Liem, L.E. and Stanley, S.J. and Smith, D.W. (1999). Turbulent velocity in flocculation by means of grids. *Journal of Environmental Engineering, ASCE*, **125**(3), 224–233.

Oldsue, J.Y. (1983). *Fluid Mixing Technology*, McGraw-Hill Book Co., New York, USA.

Park, N.S. (2002). *A Study on Distribution of Local Velocity Gradients in Rapid Mixers and Application of Hydraulic Similarity to Jar-Test*. PhD Thesis, KAIST, Korea.

Park, N.S. and Park, H. (2002). Application of hydraulic similarity to jar-tests using Froude number. *Water Research*, submitted.

Park, N.S., Park, H. and Kim, J.S. (2003). Examining the effects of hydraulic turbulence in rapid mixer on turbidity removal with CFD simulation and PIV analysis. *Journal of Water Supply: Research and Technology – AQUA* (in press).

Purchas, D.B. (1977). *Solid-Liquid Separation Equipment Scale-up*, Uplands press, Croydon, UK.

Rajendran, V.P. and Patel, V.C. (2000). Measurement of vortices in model pump-intake bay by PIV. *Journal of Hydraulic Engineering, ASCE*, **126**(5), 322–334.

Stanley, S.J. and Smith, D.W. (1995). Measurement of turbulent flow in standard jar apparatus. *Journal of Environmental Engineering, ASCE*, **121**(12), 902–910.

Wu, H. and Patterson, G.K. (1989). Laser-doppler measurement of turbulent-flow parameters in a stirred mixer. *Chemical Engineering and Science*, **44**(10), 2207–2221.

Downloaded from http://iwaponline.com/ws/article-pdf/2/5-6/47/407882/47.pdf
by guest